KSME

Springer

Journal of Mechanical Science and Technology 35 (12) 2021

Original Article
DOI 10.1007/s12206-021-1114-y

Keywords:
· Dental composite resin
· Digital image correlation
· Shrinkage strain distribution
· Principal tensile stress
· Finite element analysis

Correspondence to:
Nak-Sam Choi
nschoi@hanyang.ac.kr

Citation:
Park, J.-H., Choi, N.-S. (2021). Polymerization shrinkage and stress analysis during dental restoration observed by digital image correlation method. Journal of Mechanical Science and Technology 35 (12) (2021) 5435~5444.
http://doi.org/10.1007/s12206-021-1114-y

Received April 1st, 2021
Revised October 2nd, 2021
Accepted October 28th, 2021

† Recommended by Editor Chongdu Cho

Polymerization shrinkage and stress analysis during dental restoration observed by digital image correlation method

Jung-Hoon Park[1] and Nak-Sam Choi[2]

[1]Department of Mechanical Engineering, Graduate School, Hanyang University, Seoul 04763, Korea, [2]Department of Mechanical Engineering, Hanyang University, Gyeonggi-do 15588, Korea

Abstract Mechanistic polymerization shrinkage and stress behaviors of dental composite resins Filtek P90 (3M ESPE, USA) and Clearfil AP-X (Kuraray, Japan) were investigated using CCD camera and digital image correlation (DIC) method during and after light irradiation. For both resins, the interior of the resin part exhibited greater radial shrinkage strain (ε_r) due to more mobility than the resin margin near the interface of the substrate ring, where a non-symmetric distribution of ε_r was observed with a peak away from the center. DIC experiments on the specimen surface showed that the maximum principal stresses obtained along the margin were 1.5-8.4 times larger than the corresponding values by FEM. The non-symmetric shrinkage and the large shrinkage rate during light irradiation caused a significant increase in the principal tensile stress along the interface at cured state.

1. Introduction

Dental composite resins contain the photo-initiator camphorquinone in their molecular structure, which initiates a polymerization reaction under light stimulation. Polymerization shrinkage of the composite resin occurs due to covalent bonding of the monomers in the polymerization reaction. The shrinkage of the restoration creates a tensile stress at the interface with the tooth substrate. If the tensile stress is greater than the bonding strength, there is a high probability of interfacial defects occurring between the composite resin part and tooth substrate. Foreign substances can get intermingled into the defect space between the restoration and dentine microstructure, thus forming secondary caries and tooth fracture, which significantly reduce restored tooth life [1-3] and lead to hyper-sensitivity in patients who underwent dental restoration treatment.

The requirements for dental composite resins are specified in ISO and ANSI/ADA No. 27, where standards for biocompatibility as well as physical and chemical properties such as flexural strength, polymerization depth, water absorption, and solubility are established. The polymerization depth must be within 2 mm from the light irradiated surface and not be more than 0.5 mm different from the manufacturer's standard depth. The flexural strength related to the fracture requires more than 50 MPa after passing 24 hours of restoration treatment. These standards were established on the basis of properties of composite resins after the completion of curing; however, there is still no standard for analyzing and evaluating the shrinkage behavior occurring during resin curing.

As a method of measuring the polymerization shrinkage of composite resins, a dilatometer that measures the change in the resin volume using mercury is employed [4]. This method reacts sensitively to ambient temperature changes and yields errors due to the water absorption characteristics of the composite resin itself when calculating the polymerization shrinkage volume of the composite resin. The LVDT transducer method determines the polymerization shrinkage by placing a thin cover glass on the resin and measuring the deflection generated

during curing through an LVDT transducer. Depending on the aspect ratio of the resin sample, the measured value can be up to three times the linear shrinkage, which indicates the need for an accurate correction method [5]. The linometer method devised by Feilzer et al. [6] is a simple method for the comparison of shrinkage between resin materials; however, it is affected by the stress generated between the substrate disk and the resin specimen [7]. These methods for measuring the shrinkage strain of the composite resin were employed to measure the free shrinkage of the entire resin and did not consider local shrinkage differences. The amount of free volume change of the entire resin can differ significantly from the localized polymerization shrinkage occurring around the interface with the actual cavity in the tooth [8]. The size and direction distributions of the normal shrinkage strains during the polymerization process of composite resins can differ depending on the shape of the cavity, as they are substantially affected by the polymerization rate and boundary conditions [9, 10].

The digital image correlation (DIC) method is a non-contact observation technique that measures the deformation state over the entire surface of the projected object [11]. DIC analysis calculates the degree of brightness of each pixel in a picture with a correlation function before and after deformation, taken with a digital camera, and tracks the point with the greatest correlation, measuring the deformation and movement to calculate strain distribution. Thus, the DIC method can measure local shrinkage behaviors during the polymerization of composite resins. Through DIC analysis, Li et al. [12] confirmed that the accuracy of the shrinkage measurement differed depending on the size of the subset window, the size of the pattern particles, the intensity of the light source, and the depth of the resin. The shrinkage behavior of composite resins was addressed in a study by Chuang et al. [13] along with the stress of composite resins acting on teeth after light irradiation. The authors employed the finite element method and applied DIC results to the analysis. Vesna et al. [14] analyzed the local behavior of dental composite resins using a 3D DIC method and showed that the shrinkage strain of the composite resins was non-uniform depending on the location. Furukawa et al. [15] observed the polymerization shrinkage behavior of composite resins for various types of cavities. Li et al. [16] and Lau te al. [17] used bar specimens of composite resins and investigated the full-field 2D shrinkage strain shrinkage and shrinkage kinetics with respect to specimen depth and time. Miletic et al. [18] and Yoon et al. [19] studied local shrinkage patterns of various composites in a substrate specimen using 2D and 3D DIC and quantitatively showed in-plane complex local shrinkage patterns of the outer surface segments and out-of-plane shrinkage of the inner segments. However, these studies have rarely analyzed the observed local polymerization shrinkage and stress rising behavior of the composite resin around the marginal interface with the substrate as a function of curing time from the start of light irradiation to the curing completion.

In this study, Filtek P90 (3M ESPE, USA) and AP-X (Kuraray, Japan) dental resins with significantly different shrinkage strains are used for the test of restoration into a ring-shaped substrate. Filtek P90 a low-shrinkage silorane-based composite chosen for most restorations [20, 21] is adopted. AP-X a clinically successful methacrylate-based composite [22] is also selected for comparison. DIC is applied for the observation of shrinkage deformation behavior of the resins for dental restoration during and after light irradiation. A preliminary test enables the determination of optimum exposure times to perform actual experiment with an identical specimen under adequate photography conditions during and after light irradiation. The non-uniform distribution of shrinkage deformation of the composite resin lump restored in the substrate ring during and after light irradiation, and the drastic increase in tensile strain near the margin interface, are visualized in the full-field by DIC measurements. The strain distribution results are converted to the principal stress distribution characteristics utilizing an equivalent modulus of elasticity, and they are compared with the principal stress distribution calculated through finite element analysis [23-29] assuming a uniform shrinkage.

Table 1. Characteristics of dental composites used in this study [30].

Composite	Resin matrix	Filler	Shrinkage (vol.%)
Filtek P90	Silorane	0.01-3.5 μm (average 0.47 μm) quartz particles, yttrium fluoride (76 wt%)	-0.88
Clearfil AP-X	Bis-GMA TEDGMA	3 μm barium glass, silica particle (85.5 wt%)	-1.9

2. Methods

2.1 Specimen preparation

Two types of composite resin were used in this study: Clearfil AP-X of methacrylate disposition and Filteck P90 of silorane series. As illustrated in Table 1, the polymerization shrinkage of P90 was half that of AP-X, which were provided as trademarks by each composite resin manufacturer.

A ring type substrate was used to measure polymerization shrinkage behaviors of the composite resins. The ring substrate with 6 mm outer diameter, 4 mm inner diameter, and 2 mm height was made of polymethylmethacrylate (PMMA), which easily adhered to the dental composite resin. After cleaning of the ring substrate, the adhesive resin was applied to the inner wall of the ring substrate using a micro brush and dried by air. Light irradiation was conducted for 10 s to partially cure the adhesive layer with a light-emitting diode (LED) irradiator (1000 mW/cm^2, Morita Pencure, Japan). Subsequently, the composite resin was completely filled inside the ring from the bottom to the upper surface. The resin surface was compacted to be flat. Aqueous black paint was sprayed with fine particles onto the specimen surface using an air spray to prepare random patterning for DIC analysis.

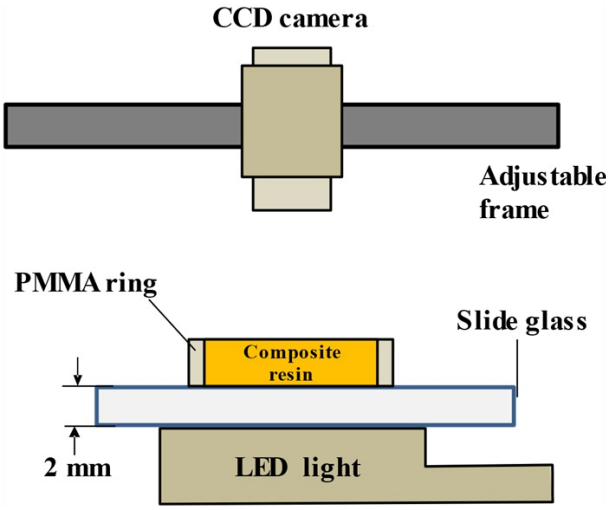

Fig. 1. Schematic of experimental imaging setup.

2.2 Dental restoration and digital image correlation analysis

Through DIC, the deformation distribution was calculated in the full-field by comparing the images of surface stain patterns before and after deformation based on the random pattern of the material surface [31, 32]. As Illustrated in Fig. 1, the LED head was maintained at a distance of 2 mm from the bottom of the specimen during irradiation. The LED head had an emitting plane area with a diameter of 9 mm which was much larger than the diameter of the substrate ring to avoid the local light effect on the resin polymerization. The light irradiation was conducted at an intensity of 1000 W for 20 s, which was sufficient for complete curing the adopted dental resins [33, 34] and common for clinical use. Digital images of polymerization shrinkage distribution were measured using the DIC camera system (ARAMIS 2M LT, GOM, Germany). Because the intensity of LED light during light irradiation and the intensity of indoor lighting after light irradiation were drastically different, the optimal shooting condition for each case was measured through preliminary tests. The exposure time during light irradiation was increased by 0.05 ms from 0.15 ms to 0.55 ms, and nine steps were taken as a variable to select the best exposure time condition for DIC analysis. The acquired image was composed of 1624×1236 pixels. The image acquisition conditions were as follows: the facet size in the image: 17×17 pixels, the facet step: 8×8 pixels, and the facet number: 321×244, the overlap area: 53 %.

By adoption of the imaging conditions described above, the non-uniform shrinkage process of the tooth restoration as a function of time was measured in the full field during light irradiation. The average radial shrinkage deformation of the composite resin at some distance from the specimen center was quantitatively calculated by Eq. (1), considering the radius variation Δr as illustrated in Fig. 2: the average radial shrinkage strain ($\overline{\varepsilon_r}$) measured through the DIC instrument ARAMIS was

Table 2. Material properties of composite resins and PMMA ring used for FE calculation.

Properties	Filtek P90		Clearfil AP-X		PMMA
	Resin	Bond	Resin	Bond	
Elastic modulus [MPa]	153 (equivalent)	2300	186 (equivalent)	4400	3200
Poisson's ratio	0.3	0.3	0.26	0.24	0.3
Polymerization shrinkage [vol.%]	-0.88	-	-1.9	-	-

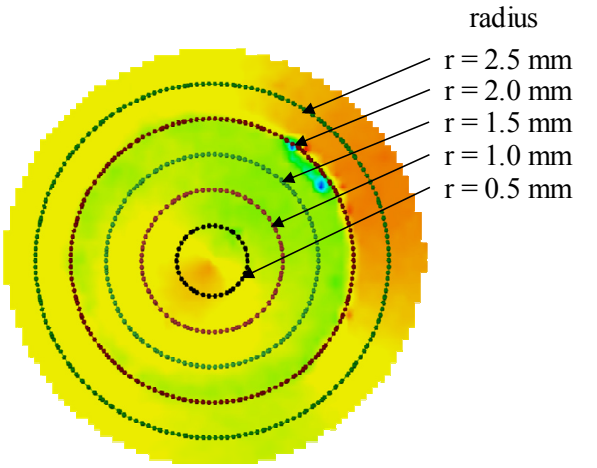

Fig. 2. Top-view image of a restoration ring substrate specimen, and circumferences according to five radial distances from the center to calculate average shrinkage strains on the specimen surface.

obtained for the circumference at each location of radius by 0.5 mm intervals from the specimen center.

$$\overline{\varepsilon_r} = \frac{1}{N}\sum_{i=1}^{N}\left(\frac{\Delta r_i}{r_i}\right) \quad (1)$$

Here, r_i is the radial distance from the center, and Δr_i is the displacement of the specified location at dividing the circumference by N equal parts, in which the corresponding radial distance r_i is a constant value along the circumference. The circumference was equally divided (N), for instance, when r = 0.5 mm, N = 46; r = 1.0 mm, N = 94; r = 1.5 mm, N = 142; r = 2.0 mm, N = 184; and r = 2.5 mm, N = 234.

2.3 Finite element stress analysis

The principal stress distribution on the surface of the specimen was calculated on the basis of the FEM three-dimensional model shown in Fig. 3. An equivalent elastic modulus was obtained beforehand [35] for the composite resin subjected to the entire curing process, and it was applied to the FEM model. The FE mesh represents an axi-symmetric quarter model of the actual specimen consisting of 2280 elements and 7175 node points. The interface between the composite resin, adhe-

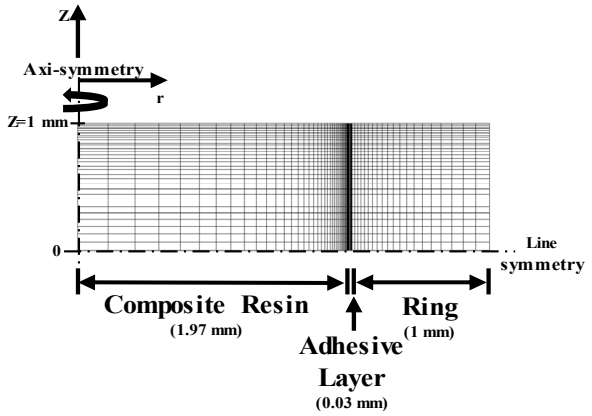

Fig. 3. Modeling of a dental restoration ring for 3D finite element calculation.

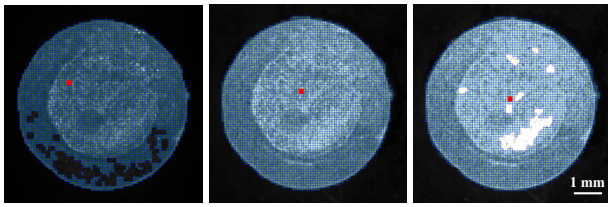

Fig. 4. Photograph images acquired for DIC according to various camera exposure times.

sive layer, and outer ring was assumed to have a perfect bonding condition, and the Poisson's ratio and linear shrinkage assumed in FEM are shown in Table 2. Mechanical property values except the elastic modulus in Table 2 were based on the cured state and did not reflect the change in behavior of the gel state over time. A constant linear shrinkage strain of the composite resin part in the substrate ring was applied to the model by equivalence to the heat shrinkage strain according to a temperature decrease [36]. The normal stresses in the radial direction on the surface of the FE model were calculated from the center of the specimen to the resin-adhesive interface (r = 1.97 mm).

3. Results

Fig. 4 shows a series of photographs acquired for the same restoration specimen, which were examined to determine whether the images with different camera exposure times at a light intensity of 1000 mW/cm^2 could interpret the local area of the resin. In the image, the gray-toned region depicts the area that is subject to interpretation, while the black and white local regions indicate uninterpretable aspects subjected to insufficient or excessive light, respectively. With an exposure time of 0.25 ms or less, the local area for which the intensity of light was insufficient corresponds to the PMMA substrate, whereas with an exposure time of 0.45 ms or more, several local areas of the composite resin could not be interpreted due to excessive exposure. Fig. 5 shows the percentage of the interpretable area as a function of exposure time against the total target area,

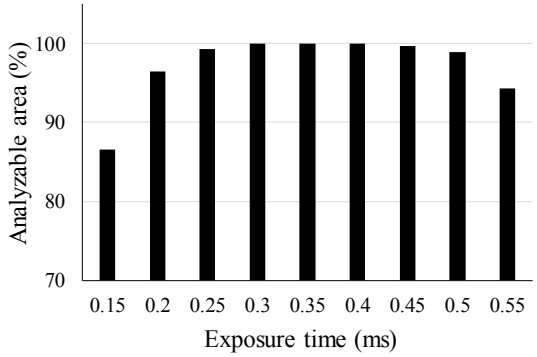

Fig. 5. Percentages of analyzable area according to various exposure times.

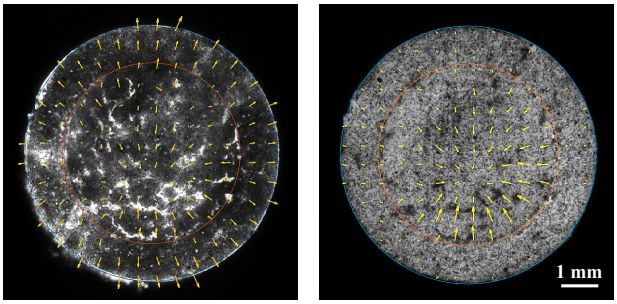

Fig. 6. Displacement vector distribution of a composite resin-filled ring specimen for P90 measured by DIC: (a) just before the completion of light irradiation; (b) at a cured state for 10 min. The arrows in the picture indicate displacement vectors six times enlarged to facilitate visual observation.

which was divided into micro-areas for image quality analysis. When the exposure time changed from 0.15 to 0.25 ms, the area that could be interpreted changed from 87 to 99 %, respectively. In the case of 0.30 to 0.40 ms exposure time, the analysis was possible in all micro-areas. However, the analyzable area deteriorated from 99 to 94 % at exposure times longer than 0.45 ms. Therefore, a short exposure time of 0.30 ms was set as the optimal acquisition condition for the process of light irradiation. After completing light irradiation, the optimal exposure time of 300 ms was adopted for under indoor lighting in the laboratory.

Figs. 6(a) and (b) show photographs taken just before the completion of light irradiation of the P90 specimen for 20 s and immediately after the end of the curing test for 10 min, respectively where displacement vectors measured through DIC are visualized together on the corresponding photographs. The lengths of the arrow vectors were enlarged to six times the actual displacement vectors to facilitate observation at the corresponding locations. In the photo just before the completion of light irradiation, the central region of the resin showed high shrinkage behavior, whereas the substrate ring part and the resin margin showed some expansion behavior due to heat inflow from the light source and the polymerization exothermic reaction. The curing test continued further for nine minutes and forty seconds after the light irradiation stopped. Although there

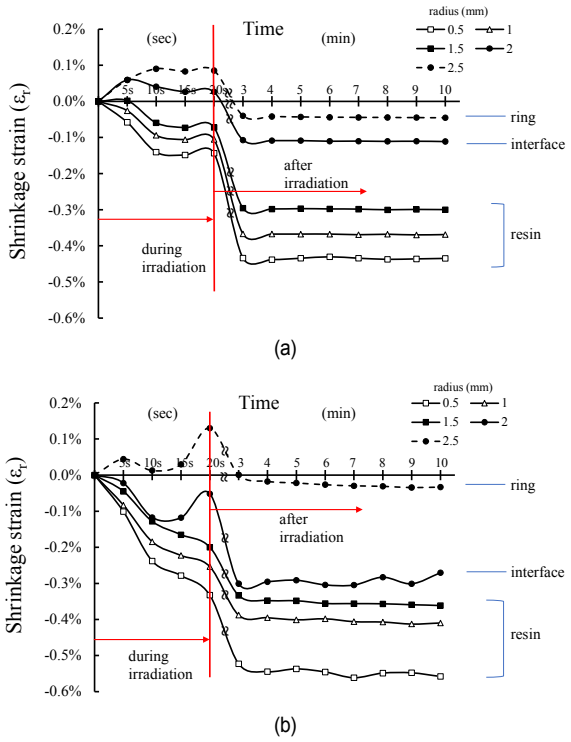

Fig. 7. Average radial shrinkage strain of (a) P90; (b) AP-X as a function of time during and after LED irradiation.

is a theoretical principle that the shrinkage should be zero at the center (r = 0) because the center location corresponds to the axi-symmetric line of the ring substrate, the actual centrality of shrinkage displacement vectors was located slightly away from the center, as shown in Figs. 6(a) and (b) from the light irradiation to the completion of the test. Such non-symmetric behavior of actual shrinkage vectors was considered to be caused by non-uniform distribution of filler particles and constituents of the resin part filled in the ring substrate. Thus, a single strong shrinkage centrality was observed at a site slightly away from the center of the resin, spreading the shrinkage over the entire surface of the specimen, as manifested in Fig. 6(b). The peak shrinkages represented by the large displacement vectors was predominantly distributed along the domain away from the resin center.

Fig. 7 shows average radial shrinkage strain ($\bar{\varepsilon}_r$) measured for each radius location r according to the elapsed time from the start of light irradiation. For the resins of P90 (Fig. 7(a)) and AP-X (Fig. 7(b)), the absolute $\bar{\varepsilon}_r$ significantly decreased as the location of radius moved from around the center of the resin (r = 0.5 mm) to the margin (r = 2.0 mm). For P90, natural shrinkage was approximated at 46 % of that of AP-X (see Table 1), but average shrinkage strain was -0.14 % at r = 0.5 mm just before the end of light irradiation for 20 s. It was rather expanded to +0.08 % at r = 2.5 mm in the substrate ring of PMMA and to +0.02 % at r = 2.0 mm at the margin of resin due to thermal expansion by heat inflow received from the light source and by the exothermic resin reaction. At ~3 min after

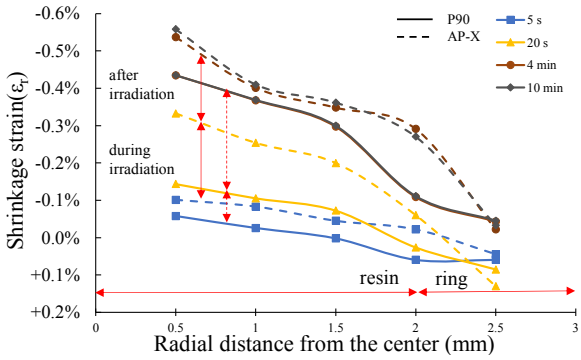

Fig. 8. Comparison of average radial shrinkage strain for P90 and AP-X according to radial distances from the specimen center.

the irradiation, the polymerization shrinkage deformation was shown as almost completed. At the end of the curing test at 10 min, $\bar{\varepsilon}_r$ was at the maximum to be -0.43 % at r = 0.5 mm, exhibiting a peak shrinkage, whereas it was very low to be around -0.04 % at r = 2.5 mm.

For AP-X (Fig. 7(b)) just before the end of light irradiation, $\bar{\varepsilon}_r$ of the central region at r = 0.5 mm was -0.33 %, the absolute of which exhibited a higher shrinkage strain than P90. The margin of the resin around r = 2.0 mm showed a small shrinkage with a large variation, which was very different from the expansion behavior of P90. It seems that the polymerization shrinkage rate of AP-X during the light irradiation was much higher than the thermal expansion amount induced by heat inflow from the light source and the exothermic reaction of resin itself. Approximately 90 % of the polymerization shrinkage was completed at 3 min of elapsed time after light irradiation start. At 10 min, the average value of ε_r at r = 0.5 mm reached -0.56 %, which showed the largest radial shrinkage strain over the surface. The resin margin at r = 2.0 mm likewise experienced a significant shrinkage deformation of -0.30 %.

Fig. 8 shows changing behavior of the average radial shrinkage strain $\bar{\varepsilon}_r$ calculated according to the r distance from the center. Just after 5 s from the initial irradiation, as the r distance increased from 0.5 to 2.5 mm, $\bar{\varepsilon}_r$ for AP-X and P90 changed from -0.10 to +0.04 %, and -0.058 to +0.05 %, respectively. The ε_r was distributed with a shrinkage state in the resin part, and an expansion in the substrate ring.

At 10 min of elapsed time after the completion of irradiation, $\bar{\varepsilon}_r$ of AP-X decreased from -0.56 % to a remarkably small value of -0.03 % as the r distance increased 0.5 to 2.5 mm, whereas P90 showed a small increase from -0.43 to -0.05 %. AP-X experienced a large shrinkage strain during the light irradiation of 20 s, whereas P90 contracted the most after the light irradiation. The amount of shrinkage proceeded during the light irradiation was significantly different depending on the resin.

Fig. 9 shows the distribution of the first principal strain (ε_1) measured on the surface through DIC analysis just after the curing test of 10 min for AP-X and P90 under the same experimental conditions. The ε_1 was calculated by Eq. (2)

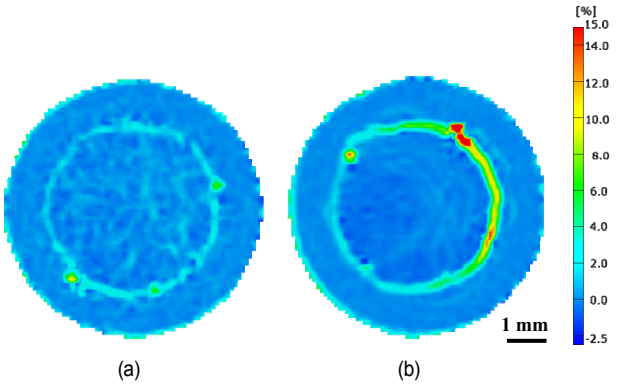

Fig. 9. Principal strain (ε_1) distributions measured by DIC on cured specimen surface for (a) P90; (b) AP-X.

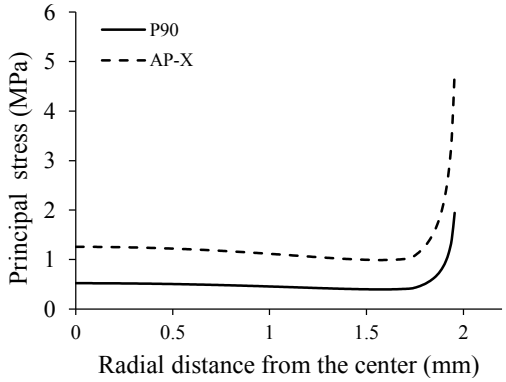

Fig. 10. Principal stress (σ_1) distribution calculated through FEM on the surface of composite resin part in a ring substrate with respect to radial distance from the center.

through the normal strains in the x direction (ε_x) and the y direction (ε_y), and the shear strain (γ_{xy}), which were measured by DIC at each location on the specimen surface.

$$\varepsilon_1 = \frac{\varepsilon_x + \varepsilon_y}{2} + \frac{1}{2}\sqrt{\left(\varepsilon_x - \varepsilon_y\right)^2 + \gamma_{xy}{}^2} \quad (2)$$

For AP-X, ε_1 showed a highly non-uniform distribution across the specimen surface, where the margin of the resin near the interface (r = 2 mm) showed remarkably large values of 4.0-21.6 % of the tensile mode. The large values of ε_1 concentrated around the interface and distributed a strong bias to one side with a non-symmetry pattern along the circumferential interface. This behavior was very compared to the low values of -2.5 to +2 % around the central region. For P90, values of ε_1 along the resin margin were distributed to be ~2.0 to +10 % in tension, which was also substantially larger than in the central region.

Fig. 10 shows distribution of the first principal stress (σ_1) on the specimen surface with respect to the r location from the center. σ_1 was calculated through the three-dimensional FE model by applying the equivalent modulus of elasticity (AP-X: 186 MPa, P90: 153 MPa) obtained in Ref. [35]. The first principal stress was almost the same as the radial normal stress σ_r because of the axi-symmetric geometry of the resin part. As a result of the FEM calculation, the shrinkage by the resin polymerization showed the deformation behavior of a concave shape near the interface between PMMA ring and the resin part, where the tensile σ_1 was highly concentrated on the margin of the resin part. The distribution behavior of σ_1 was basically similar to that of ε_1 in Fig. 9. The large principal stress, i.e., the large tensile stress in the radial direction, can cause tensile delamination or cracking along the interface in a state subjected to the principal tensile strain concentrated around the interface.

4. Discussion

The shrinkage deformation of the composite resin for the tooth restoration model, analyzed by DIC, confirmed that the shrinkage strain was significantly different at the center and margins of the resin part (Fig. 8). This non-uniform shrinkage strain distribution of the resin part is attributed to the difference in the local curing speed: The light-receiving efficiency at the marginal portion of the resin adjacent to the substrate wall boundary was lower, and thus the polymerization speed was slower than that of the resin center when the resin part was irradiated by external uniform lighting. The resin progressively undergoes a phase change [37] from the initial sol to the gel state, such that the flowability disappears. The polymerization shrinkage rate of the resin was the largest at the center and slowest along the margins. This behavior continued throughout the duration of light irradiation. After entering the gel state, an elastic contraction force occurred in the resin part, and the balanced spring reaction force [19] of the substrate ring intensively raised the tensile stress around the resin margin, as shown in Fig. 10.

In Fig. 7, the average ε_r was obtained at 0.5 mm intervals from the center on the specimen surface. During light irradiation, the average ε_r of each resin definitely decreased with less shrinkage as the r distance progressed toward the margin. In contrast, closer to the center, a larger radial shrinkage strain occurred because the resin of the central region had a high rate in polymerization shrinkage than the margin as stated above. In the resin part (r < 2.0 mm) during the initial 20 s of light irradiation, AP-X showed that 50-60 % of the total shrinkage strain throughout the curing test arose in the irradiation period. For P90, a comparatively small percentage (23-35 %) of the total shrinkage occurred in that period.

The line shrinkage strains of AP-X and P90 in the free resin state measured by the authors [28] through the bonded disk method [38, 39] were -0.70 and -0.37 %, respectively (approximately 1/3 of the corresponding volume strain values in Table 1). The present shrinkage strains of -0.27 and -0.11 % at r = 2.0 mm measured in this experiment are only approximately 1/3 of the above free line shrinkage. This is mainly attributed to the local flow behavior of the resin in the initial sol state. During the initial 20 s of light irradiation, the central region of the specimen contracts substantially more than the resin margin fixed at

the inner wall surface of the ring substrate. In contrast, the shrinkage strains at the interface and in the substrate ring were small, and the resin shrinkage generated a tensional contraction force on the inner wall of the substrate ring in the direction of the center. The contraction force caused the concentration of the principal tensile stress along the margin of the resin, as illustrated in Fig. 10. Because of the offset effect of the tensional contraction force, the resin shrinkage by light irradiation became largely relaxed around the margin and converted to principal tensile strains, confirmed in Fig. 9. The contraction force caused considerable compressive circumferential strains distributed in the substrate ring, which are explained in a mechanical analysis of Ref. [35].

To calculate the radial normal stress (σ_r) in the resin, the following stress-strain conversion Eq. (3) must be employed. The true normal strain is obtained by subtracting the average normal strain $\bar{\varepsilon}_g$ (P90: 0.01 %, AP-X: -0.01 % at the margin in Fig. 7(a)) at the starting point of the gel state (P90: 35.2 s, AP-X: 11.7 s) [35] from each value of ε_r (P90: -0.11 %, AP-X: -0.27 %) measured at the margin, because the true strain must exclude the initial displacement in the sol state from the measured ε_r at the completion of curing.

$$\sigma_r = E_e \cdot \left(\varepsilon_r - \bar{\varepsilon}_g \right) \tag{3}$$

where E_e is the equivalent elastic modulus of each resin [35]. By this calculation, a tensile stress of 0.18 MPa for P90 and 0.48 MPa for AP-X acted on the margin along the interface immediately after the initial 20 s of irradiation.

In the substrate ring (r = 2.5 mm), the deformation increased in the positive direction at the initial stage of light irradiation. This behavior is attributed to the thermal expansion of the resin and the substrate ring altogether under the influence of the polymerization heat and the radiant heat transfer of the LED light source. For P90, at the interface of r = 2 mm, it rapidly expanded by up to 5 s just after light irradiation, and subsequently the extent of expansion was maintained almost constant until the end of the irradiation at 20 s. Because the coefficient of thermal expansion of the PMMA ring is about twice that of the resin, the deformation at the margin can rise in the tensile direction. Silorane, a constituent of P90, can temporarily increase in volume due to the "cationic ring opening" phenomenon [40], which opens the ring-shaped molecular structure at the beginning of curing, but may countervail after 5 s due to polymerization shrinkage.

In the case of AP-X, as there is no “cationic ring opening” phenomenon, the curing shrinkage is evident from the start of the light irradiation in the resin part including the interface, and the shrinkage variation with time is attributed to unexpected fluctuations in the heat transfer environment. The average of ε_r near the interface after the curing test was about 2.5 times higher in AP-X than P90 (Fig. 7), which was almost consistent with the shrinkage strain behavior of the resins themselves provided by the manufacturer (Table 1), in that AP-X was approximately twice as high as P90. However, the average ε_r around the center of the resin (r = 0.5 mm) was significantly reduced, such that AP-X was only 1.3 times larger. In the resin part of r ≤ 1.5 mm, both resins continued to contract even after light irradiation. The shrinkage strain was almost completed after a period of 3 min.

Table 3. Average radial shrinkage strain ($\bar{\varepsilon}_r$) for P90.

Elapsed time	Distance from the center of specimen (SD)		Line shrinkage strain (C)	Percentage (%)	
	0.5 mm (A)	2 mm (B)		A/C	B/C
20 s	-0.14 (0.14) %	0.03 (0.04) %	-0.37 %	37.8	-8.1 (thermal expansion)
10 min	-0.43 (0.27) %	-0.11 (0.04) %		116.2	29.7

Table 4. Average radial shrinkage strain ($\bar{\varepsilon}_r$) for AP-X.

Elapsed time	Distance from the center of specimen (SD)		Line shrinkage strain (C)	Percentage (%)	
	0.5 mm (A)	2 mm (B)		A/C	B/C
20 s	-0.33 (0.57) %	-0.06 (0.25) %	-0.70	47.1	8.6
10 min	-0.56 (0.76) %	-0.27 (0.20) %		80	38.6

In the light irradiation of 20 s, the $\bar{\varepsilon}_r$ markedly decreased as the r location moved from the center to the margin for both resins (Fig. 8). At the end of the curing test for 10 min, the average ε_r in P90 indicates that the shrinkage strain decreased the most from 1.5 to 2.0 mm at the r location. However, in AP-X, the shrinkage strain decreased significantly, from 0.5 to 1.0 mm at the r location. At r > 1.0 mm, the decrease of shrinkage strain was quite mild. At r = 0.5 mm, $\bar{\varepsilon}_r$ generated in the light irradiation was -0.14 and -0.32 % for P90 and AP-X, respectively. $\bar{\varepsilon}_r$ measured at the end of curing test exhibited the largest shrinkage, -0.43 and -0.56 % for P90 and AP-X, respectively.

In contrast, the percentage of $\bar{\varepsilon}_r$ formed in the light irradiation time of 20 s was 33 % for P90 and 57 % for AP-X against the final $\bar{\varepsilon}_r$ value at the end of the curing test. The shrinkage rate of P90 was significantly slower than that of AP-X. This indicates that the polymerization reaction of AP-X occurred rapidly during the light irradiation. In turn, P90 shows that most of the polymerization proceeded after the light irradiation. Hence, in P90, a certain amount of time is required for the formation of cations involved in the polymerization process of silorane [41], which has a more sticky property than AP-X, and inhibits the free movement of molecular chains during the polymerization process.

The average ε_r of each resin is compared with the free line shrinkage of the resin and shown in Tables 3 and 4 for P90 and AP-X, respectively. $\bar{\varepsilon}_r$ was obtained at the time of 20 s

just before the completion of light irradiation and at 10 min of the whole curing test.

The percentages of $\bar{\varepsilon}_r$ around the center (r = 0.5 mm) and the interface (r = 2 mm) of the specimen at the light irradiation of 20 s against the corresponding free shrinkage strain of the resins are 37.8 and -8.1 % for P90, and 47.1 and 8.6 % for AP-X, respectively. The average ε_r around the center (r = 0.5 mm) at the test of 10 min came close to the free line shrinkage strain of the resin on an almost equal level 116.2 % for P90 and 80 % for AP-X as shown in Tables 3 and 4. At the interface (r = 2 mm), however, the level of $\bar{\varepsilon}_r$ of P90 and AP-X remarkably decreased to 29.7 and 38.6 %, respectively. The contraction of the resin at the margin adjacent to the ring interface causes a remarkable decrease in shrinkage compared to the center of the resin, because of a decrease in light-receiving efficiency and a balanced influence of spring-back reaction force with the substrate ring, as described above. Therefore, predicting the distribution of polymerization shrinkage strain during tooth restoration by considering only the shrinkage strain amount of the resin itself may be significantly different from the actual strain situation.

The principal strain distribution of the specimen surface in the cured state (Fig. 9) was uneven, non-symmetric, and concentrated in the bias on one side along the interface for both resins. P90 has principal strain distribution of +2 to 10.5 % in the vicinity of the interface (r = 2 mm), which is clearly larger than inside of the resin part (Fig. 9(a)). In the case of AP-X (Fig. 9(b)), the principal strain distribution is ~4 to 21.6 % along the interface (r = 2 mm), which is significantly larger than the central part. This is caused by a large concentration of tensile stress in the vicinity of the interface between the resin and the substrate due to the spring reaction force of the ring, as well as the polymerization contraction of the resin part [35]. As the shrinkage deformation proceeds in the resin part, the principal strain at the margin adjacent to the ring wall grows to a high tension level.

As shown in Fig. 10, the principal stress calculated by FEM caused a deformation of the concave shape near the interface between the substrate and the resin due to the polymerization shrinkage, and the stress was concentrated in the region adjacent to the interface. This means that when the spring-back load of the substrate ring is applied to the resin part, it generates a concentrated tensile force on the resin margin near the interface, so that interfacial debonding may be initiated. The distribution of the principal strain (Fig. 9) on the surface measured through DIC was concentrated with a high level near the interface, and is basically consistent with the phenomenon that the principal stress is concentrated along the interface as displayed through FEM.

Table 5 shows the maximum value of the principal strain measured by DIC, the maximum principal stress calculated by Eq. (3) and the maximum principal stress calculated by FEM. Eq. (3) refers to the principal stress calculated by reflecting only the principal strain of the solid-state resin that excluded the normal strain formed before the gel-point of the resin. For both P90 and AP-X, the maximum principal stress of the interfacial resin measured by DIC is significantly larger than the maximum principal stress calculated by FEM: ~1.6 to 8.3 times for P90 and ~1.5 to 8.4 times for AP-X. Further, the maximum principal stress is approximately 3.6 to 19.2 times higher for P90 and 4.2 to 22.6 times larger for AP-X than the value of contraction stress on the inner surface of the substrate ring [35], calculated from the spring-back force of the substrate. The FEM and the spring-back force theory assumed a simple symmetric ring substrate model with uniform shrinkage distribution and constant contraction force along the interface. Those large values of σ_1 at the margin measured through DIC are caused by the different radial shrinkage behaviors strongly depending on the r distance from the center, as well as non-symmetric and biased shrinkage distribution in the resin part, as shown in Figs. 7-9.

Table 5. Maximum principal strain and maximum principal stress measured through DIC, and the corresponding maximum principal stress through FEM along the resin margin near its interface with PMMA ring.

Composite	$\varepsilon_1 - \bar{\varepsilon}_g$ (%, Eq. (3)) (SD)	Max. principal stress through DIC (SD) (MPa)	Max principal stress through FEM (MPa)	Contraction stress [19] (SD) (MPa)
Filtek P90	2.0-10.5 (1.47)	3.06-16.1 (2.25)	1.94	0.84 (0.12)
Clearfil AP-X	4.0-21.6 (3.24)	7.44-40.2 (6.03)	4.80	1.78 (0.28)

5. Conclusion

In this study, the local shrinkage characteristics of the composite resin during dental restoration were investigated from the start of light irradiation to the end of the curing test. Silorane-based composite resin (P90) and methacrylate-based composite resin (Clearfil AP-X) were used as test materials. Optimum exposure times for the DIC camera system were obtained by a preliminary test under the LED light irradiation and common room lighting without LED.

As a result of our DIC analysis, the average radial shrinkage strain ($\bar{\varepsilon}_r$) of the resin in the central region was approximately 3.9 times greater for P90 and 2.1 times greater for AP-X than the marginal region of the resin. After the curing test, the maximum $\bar{\varepsilon}_r$ appeared around the center: P90 was approximately -0.43 %, and AP-X was approximately -0.56 % on average. The absolute radial shrinkage strain decreased from around the center to the margin adhered to the ring substrate. The percentage of shrinkage progress around the center for P90 during light irradiation was 33 % for 90 and 57 % for AP-X against the completed shrinkage at the test end, and indicated very different shrinkage rates for the two resins.

On the other hand the first principal strain calculated by the normal and shear strains on the resin surface showed peak values along the margin interface. For both P90 and AP-X, the maximum principal stress was thus concentrated in the vicinity of the interface: ~3.06 to 16.1 MPa for P90 and ~7.44 to 40.2 MPa for AP-X. These values were ~1.5 to 8.4 times higher

than the corresponding maximum principal stress calculated through FEM. The non-symmetric and biased shrinkage distribution and the large shrinkage percentage during the light irradiation caused a significant increase in the tensile stress along the interface at the final cured state. The possibility of the interfacial failure formation was clarified on the basis of the local shrinkage distribution characteristics of the restored composite resin, could be examined through DIC at locations along the interface with respect to curing time.

Acknowledgments

This work was supported by the National Research Foundation of Korea (NRF) grant funded by the Korean government (MSIT) (No. 2012R1A2A2A02010147, No. 2019R1A2C1002193).

Nomenclature

ε_r : Radial shrinkage strain
Δr : Radius variation
$\overline{\varepsilon_r}$: Average radial shrinkage strain
r_i : Radial distance from the center
Δr_i : Displacement of the specified location
ε_1 : The first principal strain
ε_x : Normal strains in the x direction
ε_y : Normal strains in the y direction
γ_{xy} : Shear strain
σ_1 : Principal stress
σ_r : Radial normal stress
$\overline{\varepsilon_g}$: Average normal strain
E_e : Equivalent elastic modulus

References

[1] J. R. Bausch, K. Langede and C. L. Davidson, Clinical significance of polymerization shrinkage of composite resins, *Journal of Prosthetic Dentistry*, 48 (1) (1982) 59-67.
[2] C. J. Kleverlaan and A. J. Feilzer, Polymerization shrinkage and contraction stress of dental resin composites, *Dental Materials*, 21 (12) (2005) 1150-1157.
[3] N. Ilie, K. H. Kunzelmann and R. Hickel, Evaluation of microtensile bond strengths of composite materials in comparison to their polymerization shrinkage, *Dental Materials*, 22 (7) (2006) 593-601.
[4] M. Iga, F. Takeshige, T. Ui, M. Torii and Y. Tsuchitani, The Relationship between polymerization shrinkage measured by a modified dilatometer and the inorganic filler content of light-cured composites, *Dental Materials*, 10 (1) (1991) 38-45.
[5] A. J. Feilzer, A. J. de Gee and C. L. Davidson, Increased wall to wall curing contraction in thin bonded resin layers, *Journal of Dental Research*, 68 (1) (1989) 48-50.
[6] S. H Park, L. Krejci and F. Lutz, A comparison of micro hardness of resin composites polymerized by plasma arc or conventional visible light curing, *Operative Dentistry*, 27 (2002) 30-37.
[7] Y. C. Chung, K. S. Min, K. M. Cho and Y. B. Cho, A study of contraction shrinkage of composite resins and ormocers with various curing thimes, *Journal of Korean Academy of Conservative Dentistry*, 28 (4) (2003) 326-333.
[8] E. Asmussen and E. C. Munksgaard, Bonding of restorative resins to dentine: status of dentine adhesives and impact on cavity design and filling techniques, *International Dental Journal*, 38 (2) (1988) 97-104.
[9] S. H. Lee, J. Chang, J. Ferracane and I. B. Lee, Influence of instrument compliance and specimen thickness on the polymerization shrinkage stress measurement of light-cured composites, *Dental Materials*, 23 (9) (2007) 1093-1100.
[10] S. H. Min, J. Ferracane and I. B. Lee, Effect of shrinkage strain, modulus, and instrument compliance on polymerization shrinkage stress of light-cured composites during the initial curing stage, *Dental Materials*, 26 (10) (2010) 1024-1033.
[11] T. P. Chu, W. F. Ranson and M. A. Sutton, Applications of digital-image-correlation techniques to experimental mechanics, *Experimental Mechanics*, 25 (3) (1985) 232-244.
[12] J. Y. Li, A. Lau and A. S. L. Fok, Application of digital image correlation to full-field measurement of shrinkage strain of dental composites, *Applied Physics and Engineering*, 14 (1) (2013) 1-10.
[13] S. F. Chuang, T. Y. Chen and C. H. Chang, Application of digital image correlation method to study dental composite shrinkage, *Strain*, 44 (3) (2008) 231-238.
[14] V. Miletic, D. Manojlovic, M. Milosevic, N. Mitrovic, T. S. Stankovic and T. Maneski, Analysis of local shrinkage patterns of self-adhering and flowable composites using 3D digital image correlation, *Quintessence International*, 42 (9) (2011) 797-804 (PMID: 21909505).
[15] T. Furukawa, K. Arakawa, Y. Morita and M. Uchino, Polymerization shrinkage behavior of light cure resin composites in cavities, *Journal of Biomechanical Science and Engineering*, 4 (3) (2009) 356-364.
[16] J. Li, A. S. L. Fok, J. Satterthwaite and D. C.Watts, Measurement of the full-field polymerization shrinkage and depth of cure of dental composites using digital image correlation, *Dental Materials*, 25 (2009) 582-588.
[17] A. Lau, J. Li, Y. C. Heo and A. Fok, A study of polymerization shrinkage kinetics using digital image correlation, *Dental Materials*, 31 (2015) 391-398.
[18] V. Miletic, M. Milosevic and T. S. Stankovic, Analysis of local shrinkage patterns of self-adhering and flowable composites using 3D digital image correlation, *Quintessence International*, 42 (9) (2011) 797-804.
[19] S. Yoon, H. J. Jung, J. C. Knowles and H. H. Lee, Digital image correlation in dental materials and related research: a review, *Dental Materials*, 37 (2021) 758-771.
[20] B.-T. Gao, H. Lin, J.-M. Han and G. Zheng, Polymerization characteristics, flexural modulus and microleakage evaluation of silorane-based and methacrylate-based composites, *American Journal of Dentistry*, 24 (2) (2011) 97-102.
[21] S. H. Mahmoud, A. K. Ali and H. A. R. Hegazi, A three-year prospective randomized study of silorane and methacrylate-

based composite restorative systems in class II restorations, *The Journal of Adhesive Dentistry*, 16 (3) (2014) 285-292.
[22] S. Kubo, H. Yokota, H. Yokota and Y. Hayashi, Three-year clinical evaluation of a flowable and a hybrid resin composite in non-carious cervical lesions, *Journal of Dentistry*, 38 (2010) 191-200.
[23] S. J. Kim, The automotive stabilizer bars prepared by the third-generation method of composite fabrications, *Functional Composites and Structures*, 1 (2) (2019) 025005.
[24] L. E. Asp, M. Johansson, G. Lindbergh, J. Xu and D. Zenkert, Structural battery composites: a review, *Functional Composites and Structures*, 1 (4) (2019) 042001.
[25] H. Y. Hwang, Debondable adhesives using shape memory fibers, *Functional Composites and Structures*, 2 (1) (2020) 015003.
[26] R. J. Nedoushan and W. R. Yu, A new auxetic structure with enhanced stiffness via stiffened elliptical perforations, *Functional Composites and Structures*, 2 (4) (2020) 045006.
[27] H. Kim and W. Ji, Thermal conductivity of a thick 3D textile composite using an RVE model with specialized thermal periodic boundary conditions, *Functional Composites and Structures,* 3 (1) (2021) 015002.
[28] M. O. H. Schutzeichel, T. Kletschkowski and H. P. Monner, Effective stiffness and thermal expansion of three-phase multifunctional polymer electrolyte coated carbon fibre composite materials, *Functional Composites and Structures,* 3 (1) (2021) 015009.
[29] D.-G. Jeong and H.-S. Seo, Study on mechanical performance of 3D printed composite material with topology shape using finite element method, *Functional Composites and Structures*, 3 (3) (2021) 035003.
[30] B. T. Gao, H. Lin, J. M. Han and G. Zheng, Polymerization characteristics, flexural modulus and microleakage evaluation of silorane-based and methacrylate-based composites, *American Journal of Dentistry*, 24 (2011) 97-102.
[31] W. H. Peters and W. F. Ranson, Digital imaging techniques in experimental stress analysis, *Optical Engineering*, 21 (1982) 427-431.
[32] H. A. Bruck, S. R. McNeill, M. A. Sutton and W. H. Peters III, Digital image correlation using newton-raphson method of partial differential correction, *Experimental Mechanics*, 29 (1989) 261-267.
[33] S. J. Yoon, J. U. Gu and N. S. Choi, Influence of curing light power and energy on shrinkage force and acoustic emission characteristics of a dental composite restoration, *American Journal of Dentistry*, 26 (5) (2013) 260-264.
[34] T. Oberholzer, C. Pameijer, S. Grobler and R. Rossouw, Effect of power density on shrinkage of dental resin materials, *Operative Dentistry*, 28 (5) (2003) 622-627.
[35] J. H. Park and N. S. Choi, Equivalent Young's modulus of composite resin for simulation of stress during dental restoration, *Dental Materials*, 33 (2) (2017) e79-e85.
[36] F. P. Rodrigues, N. Silikas, D. C. Watts and R. Y. Ballester, Finite element analysis of bonded model class I 'restorations' after shrinkage, *Dental Materials*, 28 (2) (2012) 123-132.
[37] R. L. Sakaguchi, M. C. Peters, R. B. Nelson, W. H. Douglas and H. W. Poort, Effects of polymerization contraction in composite restorations, *Journal of Dentistry*, 20 (3) (1992) 178-182.
[38] D. C. Watts and A. J. Cash, Determination of polymerization shrinkage kinetics in visible-light-cured materials-methods development, *Dental Materials*, 7 (1991) 281-287.
[39] I. B. Lee, B. H. Cho, H. H. Son, C. M. Um and B. S. Lim, The effect of consistency, specimen geometry and adhesion on the axial polymerization shrinkage measurement of light cured composites, *Dental Materials*, 22 (2006) 1071-1079.
[40] L. Wen and S. V. Kraig, Physical properties of a new siloranebased restorative system, *Dental Materials*, 26 (4) (2010) 337-344.
[41] S. J. Ryu, J. H. Cheon and J. B. Min, Evaluation of polymerization shrinkage stress in silorane-based composites, *Korean Academy of Conservative Dentistry*, 36 (3) (2011) 188-195.

Jung-Hoon Park is working at Research Institute of Engineering and Technology, Hanyang University, Gyeonggi-do, Korea. He received his Ph.D. in mechanical engineering from Hanyang University. His research area is composite analysis and nondestructive inspection.

Nak-Sam Choi is Professor of Department of Mechanical Engineering, Hanyang University (ERICA), Korea. He received his B.S. in Mechanical Engineering from Seoul National University, Korea, his M.S. in Mechanical Engineering from KAIST, and Ph.D. in Composite Materials & Applied Mechanics from Kyushu University, Japan. His research interests include composites science, fatigue life and microstrain analysis, and nondestructive examination of advanced materials.